

Reinforcement of electroactive characteristics in polyvinylidene fluoride electrospun nanofibers by intercalation of multi-walled carbon nanotubes

Zahid Qamar¹ · M. Zakria² · Rana Iqtidar Shakoor³ · Muhammad Raffi² · Mazhar Mehmood⁴ · A. Mahmood²

Received: 26 August 2016 / Accepted: 2 February 2017 / Published online: 16 February 2017
© Springer Science+Business Media Dordrecht 2017

Abstract This research work reports on development and characterization of multi-walled carbon nanotube (MWCNT)-doped polyvinylidene difluoride (PVDF) nanofibers by the electrospinning method. PVDF is an extensively studied polymer both theoretically and experimentally due to its appealing ferroelectric, piezoelectric, and pyroelectric properties which strongly favors its promising applications in the development of micro/nanostructure devices. The foremost reason for its ferroelectric and piezoelectric behaviors has been attributed to its crystalline structure, specifically the presence of β -phase; however, the existence of the small percentage of β -phase in pristine PVDF limits its applications. To enhance the electroactive features in the PVDF, MWCNTs have been doped in it to prepare electrospun nanofibers, as electrospinning is a single-step approach. These nonwoven nanofibers were prepared at a DC voltage of 20 kV which were subsequently calcined at 100 °C for 12 h. The estimation of crystal structure and phase identification in these nanofibers have been determined by attenuated FT-IR and XRD, while the morphology, microstructure, mean diameter, and length have been examined by FE-SEM. The observed electrical

conductivity, capacitance, permittivity (ϵ), conductivity (δ), and impedance (Z) in these samples have been tailored by doping a range of MWCNT contents and optimizing the experimental conditions.

Keywords PVDF/MWCNTs · Electroactive · Nanofibers · β -phase · Impedance spectroscopy

Introduction

Nanostructures in materials can be designed to exhibit significantly improved physical and chemical properties and are destined to become a novel discipline of materials science and engineering for innovative applications [1]. Such materials have attracted intensive interest because of their high surface to volume ratio that instills outstanding properties for potential applications in the areas of catalysis, magnetism, electronics, optics, and medicine, etc. [2]. There are a number of processing techniques being used to fabricate nanofibers which include drawing, template synthesis, phase separation, interfacial polymerization, self-assembly, and electrospinning, etc. [3–12]. Electrospinning is an established technique which is a simple but effective method to produce pristine and hybrid continuous nanofibers, with diameters ranging from micrometers down to tens of nanometers, and of a length up to the order of even centimeters. In the electrospinning process, a suspended droplet of polymer solution or melt becomes conical in shape under the influence of a strong electric field produced by DC high voltage. This droplet is charged until the electrostatic repulsion overcomes the surface tension, resulting in deployment of highly extensional flow of polymer solution forming nanofibers/nanofibrous mats. Electrospun polymer nanofibers are an important class of nanomaterials that have attracted attention in the last few years because of

✉ Muhammad Raffi
muhammad_raffi@hotmail.com

¹ Department of Physics, Federal Urdu University of Arts, Science and Technology (FUUAST), Islamabad, Pakistan

² Department of Materials Engineering, National Institute of Lasers and Optronics (NILOP), Islamabad 45650, Pakistan

³ Department of Mechatronics Engineering, Air University, Sector E-9, Islamabad, Pakistan

⁴ Department of Materials and Metallurgy, Pakistan Institute of Engineering and Applied Sciences (PIEAS), Islamabad 45650, Pakistan

their high flexibility, mechanical strength, chemical stability, and special characteristics for advanced engineering applications such as nanofibrous membranes for air and water filtration (micro- and ultrafiltration), energy harvesting and storage, biomedical and textile industries, and development of EMI (electromagnetic interference) control surfaces [13, 14]. Furthermore, electrospun nanofiber mats possess several attractive qualities such as high porosity, pore sizes ranging from tens of nanometer to several micrometers, interconnected open-pore structure, and high permeability of gases [15]. The higher porosity in the nanofiber mats enables them to have a large surface area per unit volume accessible to the liquid filtration applications and biotechnology [16]. Polyvinylidene fluoride (PVDF) is a favorable piezoelectric polymer system because of its high flexibility, biocompatibility, and low cost, demonstrating pyroelectric and ferroelectric properties [17]. These characteristics make PVDF attractive for energy conversion applications involving microelectromechanical devices, electromechanical actuators, and energy harvesters. It is a well-known fact that PVDF crystallizes into five different phases namely α , β , δ , γ , and ε that involve three different chain conformations. Among the five polymorphs, the β -phase has the largest spontaneous polarization per unit cell and thus exhibits the highest electroactive properties. A considerable volume of research has been done in order to increase the β -phase content in PVDF by applying multiple additives and processing techniques. Efforts have been made to develop nanofiber mats by intercalation and blending of organic and inorganic additives such as nanoparticles or carbon nanotubes (CNTs) in PVDF [18, 19]. CNTs are allotropes of carbon having a cylindrical nanostructure which have been constructed with a length-to-diameter ratio of up to 132,000,000:1, showing high thermal conductivity and electrical and mechanical properties that make them a promising candidate to explore applications as additives to various structured materials [20]. The electrospun nanofibers of PVDF blended with CNTs promote the formation of the β -phase directly from the solution which results into enhancement of pyroelectric and piezoelectric responses of these nanofibers over that of the pristine one. The differential scanning calorimetry (DSC) data indicated that by loading a low aspect ratio MWCNTs has resulted into a blend of α - and β -phases whereas a high concentration of CNTs revealed towards β -phase [21]. The DSC analysis showed that due to incorporation of CNTs, the crystallinity of PVDF decreased; however, the melting and crystallization temperatures increased. According to the thermogravimetric analysis (TGA), the thermal stability has been observed to decrease due to the addition of CNTs [22]. Thermal stability and molecular retraction were assessed for nanofiber mats as during electrospinning, the molecular chains of PVDF become aligned to a state of low entropy along the fiber axis. When the membranes are heated, the surface area retracts to a

random coil state of higher entropy. To observe this mechanism, membranes of pure and composite PVDF nanofibers were heated to around 170 °C, which is slightly higher than the melting peak temperature of the PVDF. Before the melting point, there is no observable retraction of the membranes, but once the crystals started to melt, the surface area of the nanofibers began to shrink due to molecular retraction of the elongated polymer chains [23].

This research work has been undertaken to synthesize MWCNT-doped PVDF conducting nonwoven nanofiber mats by electrospinning process using PVDF as the host material. PVDF was chosen because of its useful properties such as high piezoelectricity, high chemical resistance, good mechanical properties, biocompatibility, and easy electrospinnability. The structure of these nanofibers was analyzed by X-ray diffraction and Fourier transform infrared spectroscopy (FT-IR) spectroscopy techniques. The morphology of these nanofibers was characterized by using a field-emission scanning electron microscope (FE-SEM). The frequency-dependent electrical properties were determined by impedance spectroscopy. Since both incorporation of MWCNTs in PVDF and electrospinning experimental conditions help promote the formation of β -phase, therefore, investigations on the influences on polymorphism, structure and crystal orientation, morphology, and electric conductivity have been carried out.

Experimental

PVDF (M_w 71,000, Sigma-Aldrich, UK), *N,N*-dimethylacetamide (DMAc) (99.5%, Scharlau, Spain), and acetone (99%, Sigma-Aldrich, UK) were used as received. PVDF solution was prepared by dispersing the pellets in a mixture of acetone and DMAc (50/50 volume ratio). MWCNTs (NCP, Pakistan) were suspended in 0, 0.5, 1.0, 2.0, and 4.0 wt% loadings by ultrasonication in 2.0 ml of toluene (99.7%, Sigma-Aldrich, UK). MWCNT suspension was mixed slowly under stirring in the PVDF solution which remained on stirring (WiseStir, Germany) at 80 °C for 48 h. The resultant composite solution of each MWCNT weight percent loading was filled in a 1.0-ml disposable plastic syringe fitted with a 26.5-gauge metallic needle, respectively. The filled syringe was fixed on an in-house-made syringe pump (Parker Position System, USA) in such a way that the effusion rate of the solution through the needle was adjusted to 0.9 ml/h. A vertically aligned circular-shaped copper plate (diameter 20 cm) wrapped with aluminum foil was placed at a distance of 15 cm from the tip of the needle which has been used as a grounded collector for accumulation of nanofiber mats. Pristine electrospun nanofiber mats and MWCNT-loaded PVDF were prepared at 20 kV supplied by a DC power supply (DEL Electronic Corporation, USA). Afterward, all samples were heat-treated in the oven (Memmert VO-200,

Germany) at 100 °C for 12 h. The crystalline structure, morphology, and electrical properties of the developed nanofibers were characterized by XRD (Bruker D8 Advance, Germany), FT-IR (PerkinElmer Spectrum 100, USA), FE-SEM (Panalytical, Netherlands), and impedance spectroscopy (Novacontrol Technologies, Germany). All experiments were performed at room temperature.

Results and discussion

X-ray diffraction (XRD) analysis

XRD is a promising technique used to observe the structural arrangements in nanomaterials and nanofibers. XRD data has been used to observe the effect of MWCNT loadings on the evolved microstructure of PVDF nanofibers. Electrospun nanofiber samples prepared in this work have been analyzed in the 2θ range from 10° to 30°, by the diffractometer equipped with $\text{CuK}\alpha$ ($\lambda = 1.5418 \text{ \AA}$) X-ray radiation source to evaluate their electroactive phases. The three electroactive peaks of α -, β -, and γ -phases mostly appear around 20°, while α and γ only show other signatures close to 18° [24]. So the β -phase can easily be differentiated from the other two phases.

Figure 1 shows the diffraction patterns of electrospun nanofibers of pure and MWCNT-doped PVDF, which were annealed at 100 °C for 12 h to achieve high polarity and dipole moment. Diffraction peaks observed in the as-prepared MWCNT-doped PVDF nanofibers have exhibited β -phase. From the analysis of the XRD results, it is evident that the diffraction peak observed at 18.3° is of the α -phase whereas a single peak of the β -phase has appeared at 20.6°. The two diffraction peaks of (110) and (200) planes merge together at 20.26° and appears as the β -phase [24]. This behavior in these samples has been attributed to the appearance of higher contents of β -phase in PVDF nanofibers which occurs due to molecular stretching of PVDF during the electrospinning process under the influence of a strong electric field as well as post-process annealing at the glass transition temperature of the polymer. The alpha phase, however, is believed to undergo a change with the intercalation of MWCNTs in the polymer matrix. It has been noticed from the diffraction patterns that transformation of the crystalline structure took place from α to β in such a way that the character of the α -phase has also been affected by increasing the MWCNT loading. This can be perceived with clarity from Fig. 1 that intensities of diffraction peaks were declining and shifting towards higher angles with increasing MWCNT loading compared to those of pure PVDF. The decreasing trend in crystallinity with rising loading reflects that the beta phase has improved while the alpha phase has suppressed; moreover, MWCNTs have a detrimental effect on the preferred orientations of PVDF structural chains. It has been noticed from the XRD spectra that sharpness of the beta phase peak decreased with the reinforcement of MWCNT,

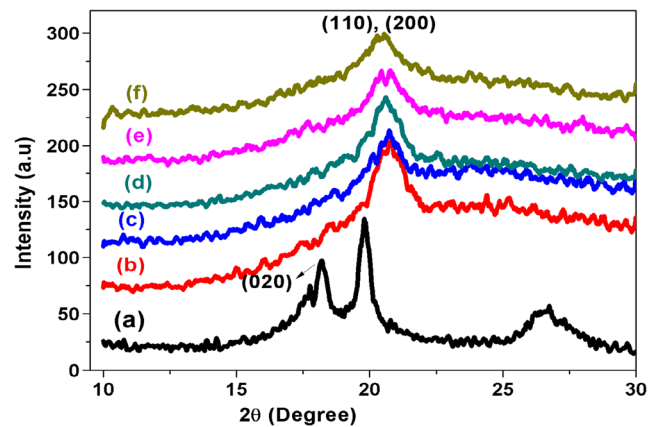


Fig. 1 XRD patterns of *a* PVDF pellet, *b* nanofibers of PVDF, *c* 0.5 wt% MWCNT:PVDF, *d* 1.0 wt% MWCNT:PVDF, *e* 2.0 wt% MWCNT:PVDF, *f* 4.0 wt% MWCNT:PVDF

which revealed that the beta phase has a higher degree of orientation. Further, broadness of the peaks and their shifting towards higher angles may be attributed to the β -phase extended-chain crystals formed under high tensile stress exerted by the electric field during the electrospinning process, because the interchain distance reduced due to stress effect [17].

FE-SEM

The effect of MWCNT doping on the morphology of electrospun PVDF nanofibers has been investigated by FE-SEM. Micrographs in Fig. 2 show that the mean diameter of nanofibers ranges between 50 and 200 nm in these nonwoven structures. From these micrographs, the diameters of these nanofibers have an increasing trend whereas the number density was noticeably falling with the addition of MWCNT loadings. The surface smoothness has decreased and waviness in the nanofibers increased with rising doping contents. As most of the MWCNTs have exhibited entangled orientations instead of alignment in preferred directions, they could not disperse uniformly, hence, becoming agglomerated within the polymer fibers. This behavior is due to the inherent dispersion characteristics of MWCNTs in the polymeric dispersions. Besides, they may not be able to stretch completely during the electrospinning process under the influence of a strong electric field [19]. The MWCNTs are more sensitive to distortions during the electrospinning process and are thus incorporated into the fibers in an entangled conformation [25].

FT-IR analysis

FT-IR spectroscopy has been conducted on these samples to examine the local conformational changes and functional groups in pristine and MWCNT-loaded PVDF nanofibers, which have taken place due to the dopant contents and exposure to the strong

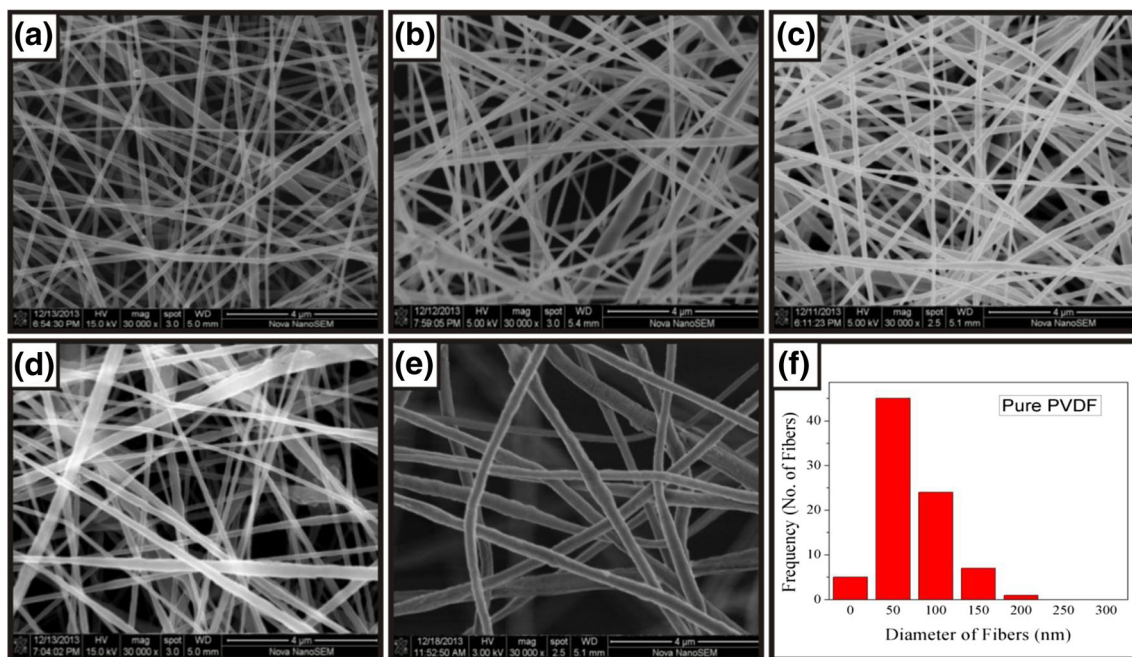


Fig. 2 FE-SEM micrographs of electrospun nanofibers. **a** Pure PVDF. **b** 0.5 wt% MWCNT:PVDF. **c** 1.0 wt% MWCNT:PVDF. **d** 2.0 wt% MWCNT:PVDF. **e** 4.0 wt% MWCNT:PVDF. **f** Mean size distribution of PVDF

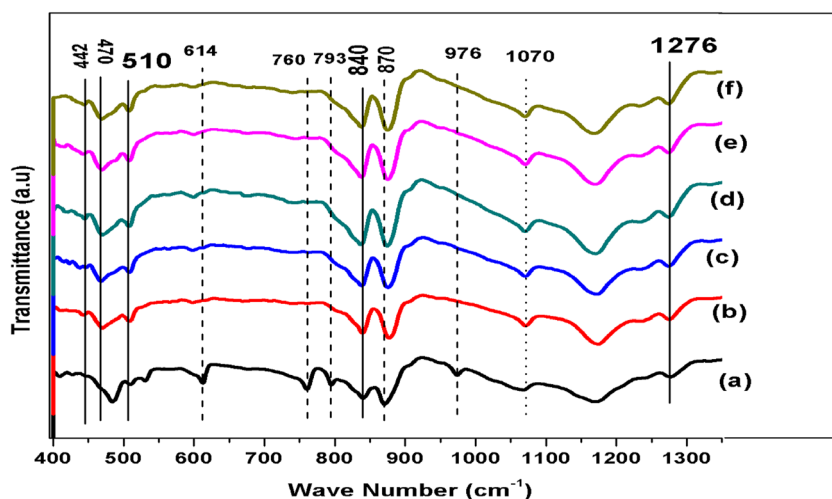
electric field during the synthesis, as well as post-synthesis annealing. In these samples, peaks of the α -phase with TGTG chain conformation have been observed at 614, 760, 793, 870, and 976 cm^{-1} respectively which are shown in Fig. 3. The distinctive peaks of β -phase with all-trans (TTTT) conformation in the MWCNT-PVDF nanofibers have been observed at 442, 470, 510, 840, and 1276 cm^{-1} , respectively. The IR absorption bands of the β -phase ($470, 840, 510,$ and 1276 cm^{-1}) have been observed to strengthen in these nanofibers with the addition of MWCNT and exposure to the strong electric field during electrospinning process [19]. The FT-IR spectra are strongly

supported by XRD analysis illustrating that the beta phase enhancement took place in the samples due to a strong interaction between π electrons of MWCNTs and fluorine (F) atoms of (TTTT) PVDF polymer chains [26].

Impedance spectroscopy

The frequency-dependent electrical transport properties introduced in the nanofibers due to the grains, grain boundary, and interfacial effects have been analyzed by complex impedance spectroscopy [27]. Usually, the electrical/dielectric response

Fig. 3 FT-IR spectra of *a* PVDF pellet, *b* PVDF nanofibers, *c* 0.5 wt% MWCNT:PVDF, *d* 1.0 wt% MWCNT:PVDF, *e* 2.0 wt% MWCNT:PVDF, *f* 4.0 wt% MWCNT:PVDF



of a material is analyzed by observing various complex electrical features like admittance (Y), permittivity (ϵ), conductivity (δ), and impedance (Z). The squared shape samples of $10 \times 10 \text{ mm}^2$ were cut from the nanofiber mats for impedance spectroscopy analysis. The wire contacts were made at the four corners of these samples by using silver paste. For this nanofiber system, real and imaginary components of complex Z , ϵ , and δ which are corresponding to a frequency range 0.1–1.0 MHz have been investigated as a function of MWCNT loading in the PVDF. The Nyquist plots shown in Fig. 4 are related to the real and imaginary components of the complex impedance Z which have been observed at different doping concentrations.

These Nyquist plots revealed that the diameters of the semi-circles have a dwindling trend with the rise of MWCNT loadings in the PVDF nanofibers. This directly reflects that charge transport conduction has enhanced due to reinforcement by addition of MWCNTs in the PVDF nanofibers [27, 28].

Figure 5 shows that real impedance (Z') values which were declining with increase in applied frequency, became nearly constant beyond 10 Hz for all concentrations of MWCNT loadings in the samples. Below 10 Hz, the value of Z' for pristine PVDF nanofibers is $4.33 \times 10^{10} \Omega$, which has been found to exhibit a decreasing trend with the rise in MWCNT loadings. The experimentally observed values of Z' in these samples have been found varied from $1.59 \times 10^{10} \Omega$ to $1.8 \times 10^8 \Omega$ for the MWCNT loadings of 0.5, 1.0, 2.0, and 4.0 wt%, respectively. It is clearly observed that Z' values have a declining trend with the rise in applied frequency, whereas its higher values at lower frequencies are attributed to the polarization caused by the creation of space charges, dipoles, ions, and electrons. At higher values of applied frequencies, higher were the orientations of the polymer molecules but only for a certain limited value. Beyond that, molecules were unable to follow the applied frequencies and would not respond any more. Such a behavior exhibited by the nanocomposite materials has been ascribed to the faster transfer rates of

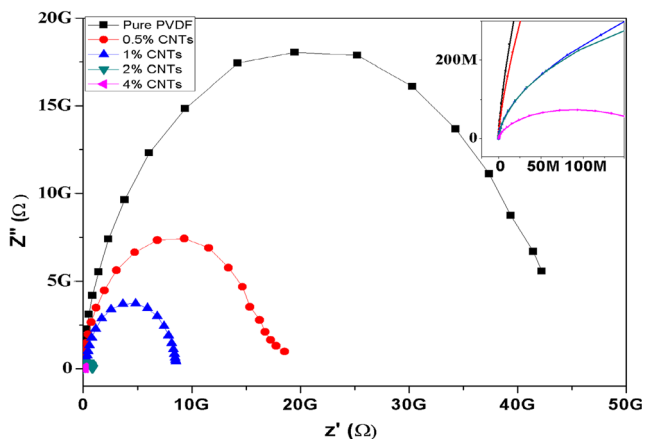


Fig. 4 Nyquist plots of pure and MWCNT-doped PVDF nanofibers

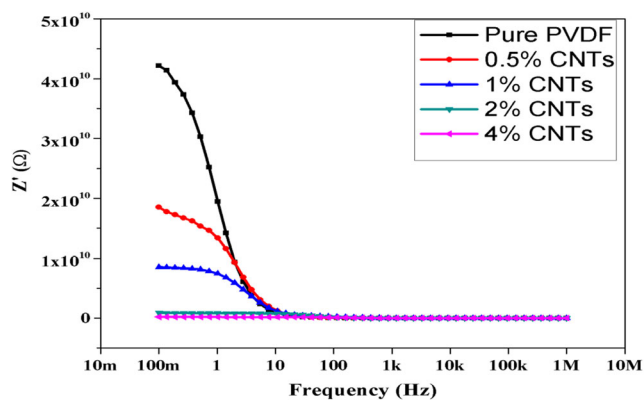


Fig. 5 Bode plot of real impedance (Z') vs frequency of pure and MWCNT doped PVDF nanofibers

the charges in these electrospun fibers, which leads to reduction of barrier properties and enhancement of alternating (AC) conductivity at higher frequencies upon increasing the MWCNT loadings [29].

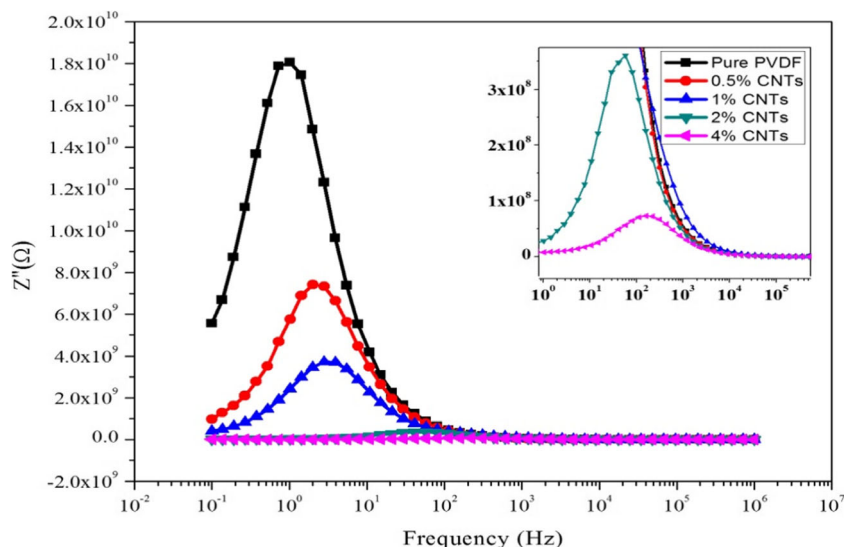
Figure 6 shows the imaginary part of the impedance (Z'') versus log of frequency for pure and loaded with different concentrations of MWCNTs in PVDF nanofibers. A relatively sharp and intense peak has been observed in the pure PVDF nanofiber mat at low frequency, i.e., 1 Hz. The peaks observed in the nanofiber mats loaded with 0.5, 1.0, 2.0, and 4.0 wt% loadings of MWCNTs have been found to be shifting towards higher frequencies which appeared at 2.4, 3.3, 50, and 160 Hz, respectively. The rising concentrations and dispersion of MWCNTs in the PVDF nanofiber mats are believed to lead to transfer of charges at a faster rate. Furthermore, these peaks have been found broadening in width and suppressing in intensity as well. These peaks are believed to be appearing in these samples due to the microphase separation of the polymer chains by the inclusion of MWCNTs. The drifting of the peak positions towards the higher frequencies also demonstrate that relaxation time was decreasing with the rising filler contents. The reduction in relaxation time in these samples is indicative of enhanced dipole density and increased polarization rates [30].

Dielectric or tangent loss is a material characteristic that does not depend on the geometrical features. Tangent loss depends on many factors and can be defined as:

$$\text{Tan } \delta = \epsilon'' / \epsilon' + \sigma / 2\pi f \epsilon' \quad (1)$$

Where, ϵ' and ϵ'' are real and imaginary components of dielectric constant, σ is the conductivity, and f is the frequency. Figure 7 reveals that dielectric losses have decreased with the increasing frequency, while it increased with the addition of MWCNT as filler in the PVDF. Here, the dielectric loss arises mainly from the excessive polarized interfaces induced by the fillers and specifically the movement of atoms or molecules by application of an alternating electric field [31, 32].

Fig. 6 Imaginary impedance (Z'') vs frequency of pure and MWCNT doped nanofibers



The increased dielectric loss with the addition of MWCNTs is the main impediment in achieving ultra-high dielectric constant because increasing the filler contents make an efficient conductive network in the polymer nanocomposite [33].

The dielectric analysis is considered an easy approach to investigate the response and behavior of polymer composites by studying the relaxation nature of dipoles of polymer electrolyte [34]. The complex dielectric permittivity can be expressed as:

$$\epsilon^* = \epsilon' - i\epsilon'' \tag{2}$$

Where, ϵ' is the real and ϵ'' is the imaginary part of the dielectric constant of the polymer electrolyte system. Moreover, the real and imaginary parts of the dielectric constant can be written as:

$$\epsilon' = C_p L / \epsilon_0 A \tag{3}$$

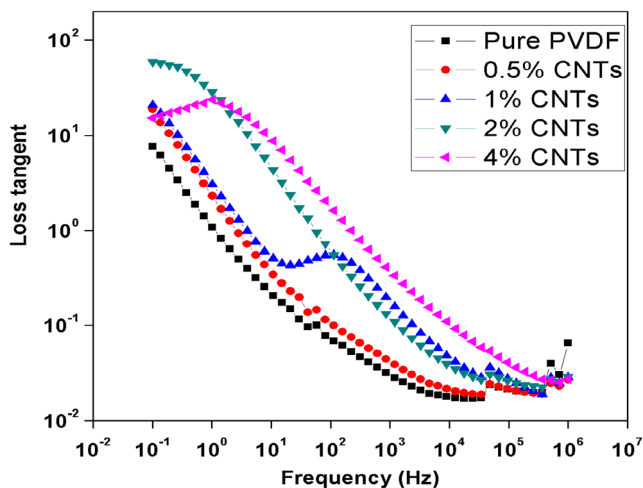


Fig. 7 Phase angle vs frequency of puer and MWCNT doped PVDF nanofibers

$$\epsilon'' = \sigma / \omega \epsilon_0 \tag{4}$$

Where, C_p is the parallel plate capacitance, L is the length, A is the area, and ϵ_0 is the permittivity of free space. Here, the real part of the dielectric constant (ϵ') is the measure of charge stored in a material, whereas imaginary part is known as a direct measurement of dissipation of energy or dielectric loss produced by the movement and effect of polarization of the charge carriers [35].

Figure 8 shows the ionic conductivity of electrospun nanofibers which has increased with the applied frequency. The conductivity of the MWCNT-doped PVDF nanofibers increased almost linearly with the frequency, showing characteristics of insulating materials [36]. At higher frequencies, MWCNTs virtually have no effect on conductivity. However, for lower frequencies, the dopant

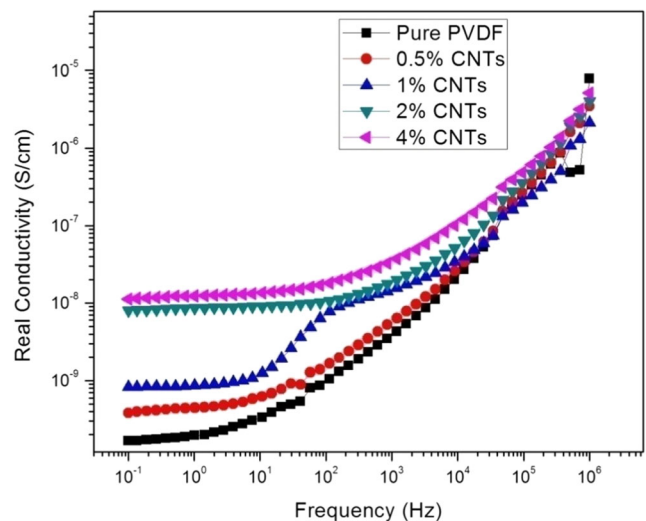


Fig. 8 Response of ionic conductivity vs frequency

effect on PVDF-nanofiber conductivity is noticeable. MWCNT doping considerably enhanced the conductivity of the target nanofibers owing to their highly conductive graphitic structures. The enhancement in conductivity was also due to the incorporation of conducting MWCNT network in the PVDF, showing percolation behavior, where the filler contents in the polymer matrix are free to move and so can make conducting paths at much lower dopant contents [37]. Further, the region of low frequency has been recognized as dispersion of charge polarization or space interfacial resistance. The amount of accumulated charges at the interface of electrode has been increased at lower the frequency region as dopant increases. As a result, the number of mobile charge carriers or ions available for the charge transportation is believed to enhance the ionic conductivity. This charge addition also specifies the existence of non-Debye properties of the polymeric composite. But, at the higher frequencies, the charge carrier mobility is greater and contributes to the higher ionic conductivity [38, 39].

It is seemingly observed from Fig. 9 that when frequency was increasing, the capacitance was decreasing; but, at higher values, it became independent of frequency. It also illustrates that data was described satisfactorily for all loadings but towards the low-frequency ends, the model deviated slightly. Therefore, by using an AC supply, a capacitor accumulates only a limited amount of charges prior to the potential difference which changes the polarity and the charge it dissipates. As the frequency increases, the less charges will be accumulated; as a result, there will be lesser opposition to the flow of current.

The overall capacitance can be calculated by the following relation:

$$C = \frac{1}{2\pi f |Z_{img}|} \tag{5}$$

Where, $|Z_{img}|$ is the magnitude of the imaginary part of the impedance in ohms; C is capacitance in F, and f is frequency in hertz. Therefore, Eq. 5 can also be rewritten as;

$$|Z_{img}| = \frac{1}{C} \omega^{-1} \tag{6}$$

Where, $\omega^{-1} = 1/2\pi f$, in radians per second. Therefore, the capacitance C can be obtained as the inverse slope of a plot of imaginary impedance Z_{imag} against the reciprocal of frequency for the low frequency data [40].

In order to study the ferroelectric properties for the PVDF-MWCNT nanofibers, the capacitance-frequency (C - F) characteristics have been studied by using an “Alpha-A High Performance Frequency Analyzer.” In Fig. 10, it is observed that the capacitance varies nonlinearly with the frequency, consequently, well-defined butterfly-shaped variations were observed in the PVDF nanofibers doped with 1.0 wt% MWCNT-loaded PVDF nanofibers, where two peaks show the two time constants. The peaks are believed to appear as a result of spontaneous polarization change, which indicates that PVDF has a ferroelectric nature. The decrease in relaxation time indicates their better energy delivery capabilities. The presence of MWCNTs in the nanofibers enhances conductance and charges carrier sites. Thus, the conductance frequency seems to be stronger with increasing MWCNT content in PVDF [41]. Moreover, a shift observed throughout the samples towards the higher frequency range has suggested that the doped MWCNTs in PVDF nanofibers contain mobile electrons or negative ions build up at the interface between the nanofibers and the electrodes [40].

Figure 11 illustrates the deviations in the dielectric constant as a function of frequency at different loadings of MWCNTs

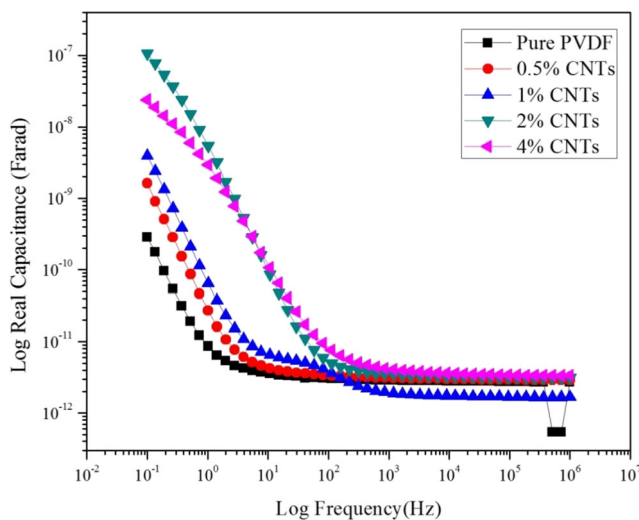


Fig. 9 Real capacitance vs frequency of pure and MWCNT doped PVDF nanofibers

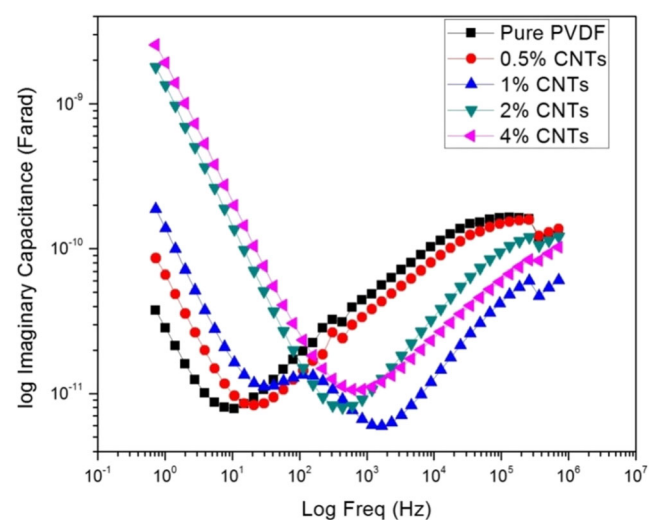


Fig. 10 Imaginary capacitance vs frequency of pure and MWCNT doped PVDF nanofibers

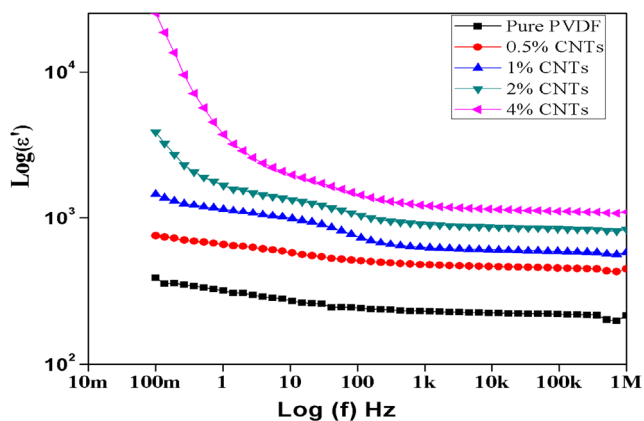


Fig. 11 Real permittivity vs frequency of pure and MWCNT doped PVDF nanofibers

in PVDF nanofibers. It has been observed from the dielectric plots that there was only one relaxation process in these nanofibers except in 1.0 wt% MWCNT loading where two relaxation processes were witnessed. The dielectric constant has been found to decrease with the rise in the frequency. This type of behavior in nanocomposites is attributed to the fact that at lower frequencies, dielectric response follows the excitation field, but as the frequency increases, these dipoles lag behind the applied field and thus reduce the dielectric constant of the material. According to the Koop's model, the dielectric in heterogeneous structures can be thought of as conducting grains with the separation of highly resistive grain boundaries. As a result, the space charge polarization builds up at the grain boundaries which govern the free charge carriers available at the grain boundaries as well as the conductivity of the material. As the grain boundaries respond at low frequencies, so higher will be the dielectric constant. This supports the values of high dielectric constant at lower frequencies. It can also be

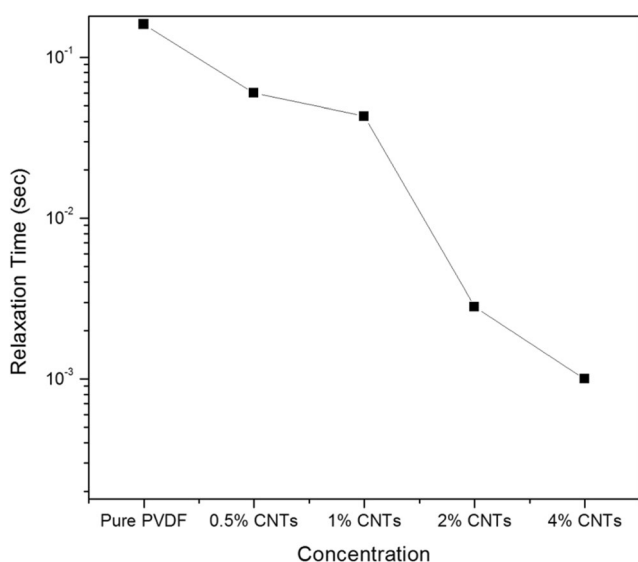


Fig. 12 Variation of relaxation time vs MWCNT loading in PVDF nanofibers

seen that the dielectric constant has strengthened with the rising contents of MWCNTs in the PVDF [35].

Figure 12 shows the variation of relaxation time as a function of MWCNT loading in PVDF nanofibers. The characteristic relaxation time (τ) was calculated from Z' and Z'' (Nyquist plot) and also from $\log(f)$ and Z'' graphs. The relaxation time is given as:

$$\tau = \frac{1}{2\pi f_{\max}} \quad (7)$$

Where, f_{\max} is the relaxation frequency at which the Z'' is found to be maximum. It is observed that by increasing the MWCNT loading in the nanofibers, the relaxation time (τ) decreased eventually, which shows the semiconducting behavior [42, 43].

Conclusions

Pure and MWCNT-loaded PVDF nanofiber mats have been synthesized by the electrospinning method. As prepared pure and MWCNT-doped nanofibers were found amorphous, crystallinity appeared after annealing in the air. The structural analysis have revealed that strong electric field and heat treatment have played a key role to foster crystallinity in these polymeric nanocomposites which resulted into formation of different phases that strongly depend upon the temperature gradients. As the electrospinning process has taken place under the influence of a strong electric field which promoted formation of the β -phase in the PVDF. The morphological analysis has revealed that MWCNTs are homogeneously dispersed in the PVDF matrix; however, while increasing the MWCNT loadings in the PVDF matrix, the diameter of the formed nanofibers has improved while beading subsided. The impedance spectroscopy has revealed that addition of MWCNTs has decreased the resistivity, which improved inherent piezoelectric effect of pure PVDF. As a result, MWCNT-doped PVDF nanofibers may require less stresses for better piezoelectric response in comparison to pure PVDF. Another characteristic is the enhancement of β -phase due to the synergistic effect of extensional forces and the reinforcement caused by MWCNTs along the chains of the PVDF nanofibers.

Acknowledgements The authors would like to sincerely thank the Department of Materials and Metallurgy, PIEAS, Islamabad for extending the support required for completion of this research work.

References

1. Roco MC, Williams RS, Alivisatos P (2000) Nanotechnology research directions: IWGN workshop report: vision for nanotechnology in the next decade, Springer Science & Business Media

2. Camargo PHC, Satyanarayana KG, Wypych F (2009) Nanocomposites: synthesis, structure, properties and new application opportunities. *Mater Res* 12:1–39 ISSN 1516-1439
3. Ahmed FA, Ali SH, Al-Masry WA, Al-Zeghaye Y (2012) Fabrication of chitosan nanofibers membrane and its treatment. *Adv Sci Lett* 17(1):217–223
4. Burger C, Hsiao BS, Chu B (2006) Nanofibrous materials and their applications. *Annu Rev Mater Res* 36:333–368
5. Ondarcuhu T, Joachim C (1998) Drawing a single nanofibre over hundreds of microns. *Europhys Lett* 42:215–220
6. Feng L, Li S, Li H, Zhai J, Song Y, Jiang L, Zhu D (2002) Superhydrophobic surface of aligned polyacrylonitrile nanofibers. *Angew Chem Int Ed* 41:1221–1223
7. Martin C (1996) Membrane-based synthesis of nanomaterials. *Chem Mater* 8:1739–1746
8. Ma P, Zhang R (1999) Synthetic nano-scale fibrous extracellular matrix. *J Biomed Mater Res* 46:60–72
9. Liu G, Ding J, Qiao L, Guo A, Dymov BP, Gleeson JT, Hashimoto T, Saijo K (1999) Polystyrene-block-poly (2-cinnamoyl ethyl methacrylate) nanofibers—preparation characterization and liquid crystalline properties. *Chem Eur J* 5:2740–2749
10. Whitesides GM, Grzybowski B (2002) Self-assembly at all scales. *Science* 295:2418–2421
11. Deitzel JM, Kleinmeyer JD, Hirvonen JK, Tan NB (2001) Controlled deposition of electrospun poly (ethylene oxide) fibers. *Polymer* 42:8163–8170
12. Bhardwaj N, Kundu SC (2010) Electrospinning: a fascinating fiber fabrication technique. *Biotechnol Adv* 28(3):325–347
13. Nirmala R, Navamathavan R, Park SJ, Kim H (2014) Recent progress on the fabrication of ultrafine polyamide-6 based nanofibers via electrospinning: a topical review. *Nano-Micro Letters* 6(2):89–107
14. Mohammadzadehmoghadam S, Dong Y, Jeffery Davies I (2015) Recent progress in electrospun nanofibers: reinforcement effect and mechanical performance. *J Polym Sci B Polym Phys* 53(17):1171–1212
15. Feng C, Khulbe KC, Matsuura T, Tabe S, Ismail AF (2013) Preparation and characterization of electro-spun nanofiber membranes and their possible applications in water treatment. *Sep Purif Technol* 102:118–135
16. Hardick O, Dods S, Stevens B, Bracewell DG (2015) Nanofiber adsorbents for high productivity continuous downstream processing. *J Biotechnol* 213:74–82
17. Huang S, Yee WA, Tjiu WC, Liu Y, Kotaki M, Boey YC, Ma J, Liu T, Lu X (2008) Electrospinning of polyvinylidene difluoride with carbon nanotubes: synergistic effects of extensional force and interfacial interaction on crystalline structures. *Langmuir* 24(23):13621–13626
18. Liu ZH, Pan CT, Lin LW, Lai HW (2013) Piezoelectric properties of PVDF/MWCNT nanofiber using near-field electrospinning. *Sensors Actuators A Phys* 193:13–24
19. Mokhtari F, Latifi M, Shamshirsaz M (2016) Electrospinning/electrospray of polyvinylidene fluoride (PVDF): piezoelectric nanofibers. *The Journal of the Textile Institute* 107(8):1037–1055
20. Xu W (2011) Carbon material based microelectromechanical system (MEMS): fabrication and devices. PhD Dissertation, Georgia Tech University, USA
21. Ma J, Haque RI, Larsen RM (2012) Crystallization and mechanical properties of functionalized single-walled carbon nanotubes/polyvinylidene fluoride composites. *J Reinf Plast Compos* 31(21):1417–1425
22. Huang X, Jiang P, Kim C, Liu F, Yin Y (2009) Influence of aspect ratio of carbon nanotubes on crystalline phases and dielectric properties of poly (vinylidene fluoride). *Eur Polym J* 45(2):377–386
23. Yu L, Cebe P (2009) Crystal polymorphism in electrospun composite nanofibers of poly (vinylidene fluoride) with nanoclay. *Polymer* 50:2133–2141
24. Martins P, Lopes AC, Lanceros-Mendez S (2014) Electroactive phases of poly (vinylidene fluoride): determination, processing and applications. *Prog Polym Sci* 39(4):683–706
25. Dror Y, Salalha W, Khalfin RL, Cohen Y, Yarin AL, Zussman E (2003) Carbon nanotubes embedded in oriented polymer nanofibers by electrospinning. *Langmuir* 19(17):7012–7020
26. Yu S, Zheng W, Yu W, Zhang Y, Jiang Q, Zhao Z (2009) Formation mechanism of β -phase in PVDF/CNT composite prepared by the sonication method. *Macromolecules* 42(22):8870–8874
27. Moharana S, Mishra MK, Behera B, Mahaling RN (2015) A comparative study of dielectric properties of calcined and un-calcined BiFeO₃-poly (vinylidene fluoride) (PVDF) composite films. *International Journal of Engineering Technology, Management and Applied Sciences* 3(4):303–315
28. Ranjan R, Kumar R, Kumar N, Behera B, Choudhary RN (2011) Impedance and electric modulus analysis of Sm-modified Pb (Zr 0.55 Ti 0.45) 1-x/4 O 3 ceramics. *J Alloys Compd* 509(22):6388–6394
29. Camargo PH, Satyanarayana KG, Wypych F (2009) Nanocomposites: synthesis, structure, properties and new application opportunities. *Mater Res* 12(1):1–39
30. Afzal AB, Akhtar MJ, Nadeem M, Hassan MU (2010) Investigation of electrical properties of polyaniline nanocomposites by impedance spectroscopy. *Key Eng Mater* 442:356–363
31. Johnson GL (2001) Inductors and transformers: the first Tesla Museum and Science Center International Conference on Nikola Tesla, Farmingville, New York, October 6–8, 2006
32. Gouda OE, Thabet AM, El-Tamaly HH (2004) How to get low dielectric losses in binary and multi-mixtures dielectrics at high frequency. *Universities Power Engineering Conference IEEE* 3: 1237–1240
33. Qi L, Lee BI, Chen S, Samuels WD, Exarhos GJ (2005) High dielectric constant silver-epoxy composites as embedded dielectrics. *Adv Mater* 17(14):1777–1781
34. Ibrahim S, Yasin SM, Nee NM, Ahmad R, Johan MR (2012) Conductivity and dielectric behaviour of PEO-based solid nanocomposite polymer electrolytes. *Solid State Commun* 152(5): 426–434
35. Katoch A, Borthakur BK, Singh A, Singh T (2013) Electrical and dielectric properties of M-type strontium hexaferrites doped with Gd-rare earth ions. *International Journal of Engineering Research and Technology* 2(3):1–6
36. Li Y, Chin Tjong S (2012) Electrical properties of binary PVDF/clay and ternary graphite-doped PVDF/clay nanocomposites. *Curr Nanosci* 8(5):732–738
37. Bauhofer W, Kovacs JZ (2009) A review and analysis of electrical percolation in carbon nanotube polymer composites. *Compos Sci Technol* 69(10):1486–1498
38. Dieterich W, Maass P (2002) Non-Debye relaxations in disordered ionic solids. *Chem Phys* 284(1):439–467
39. Khatri P, Behera B, Choudhary RN (2009) Structural and electrical properties of Sr₃V₂O₈ ceramics. *Phys Status Solidi B* 246(5): 1118–1123
40. Baumgarten PK (1971) Electrostatic spinning of acrylic microfibers. *J Colloid Interface Sci* 36(1):71–79
41. Senthilkumar ST, Selvan RK, Ulaganathan M, Melo JS (2014) Fabrication of Bi₂O₃ AC asymmetric supercapacitor with redox additive aqueous electrolyte and its improved electrochemical performances. *Electrochim Acta* 115:518–524
42. Chakraborty G, Meikap AK, Babu R, Blau WJ (2011) Activation behavior and dielectric relaxation in polyvinyl alcohol and multi-wall carbon nanotube composite films. *Solid State Commun* 151(10):754–758
43. Fan DL, Zhu FQ, Xu X, Cammarata RC, Chien CL (2012) Electronic properties of nanoentities revealed by electrically driven rotation. *Proc Natl Acad Sci* 109(24):9309–9313